Femtosecond Dynamics of Pyridine in the Condensed Phase: Valence Isomerization by Conical Intersections

2 **AUTHORS**, INCLUDING:

Mirianas Chachisvilis

61 PUBLICATIONS **2,001** CITATIONS

SEE PROFILE

Femtosecond Dynamics of Pyridine in the Condensed Phase: Valence Isomerization by Conical Intersections

Mirianas Chachisvilis[†] and Ahmed H. Zewail*

Arthur Amos Noyes Laboratory of Chemical Physics, Laboratory for Molecular Sciences,
California Institute of Technology, Pasadena, California 91125

Received: June 3, 1999

In this work, we combined femtosecond transient absorption (population and anisotropy) spectroscopy with ab initio electronic structure methods to study excited-state deactivation pathways of the pyridine molecule in liquid solutions. Studies of the effects of excitation energy, deuteration and substitution, solvent polarity and viscosity, and protonation of pyridine were performed. The experiments reveal the dynamics of $S_1(n\pi^*)$ and $S_2(\pi\pi^*)$ excited states of pyridine. The photoexcitation of the $S_2(\pi\pi^*)$ state leads to formation of the prefulvenic form of pyridine, a valence isomer, in ~2.2 ps, while nonradiative deactivation of the $S_1(n\pi^*)$ state occurs in 9–23 ps and is to a large extent due to intersystem crossing. Using ab initio methods at the CASSCF and time-dependent DFT levels, we calculated the potential energy surfaces of the ground and $S_2(\pi\pi^*)$ states. A conical intersection was found responsible for the ultrafast deactivation of the pyridine molecule.

1. Introduction

The problem of predicting the branching between energetically allowed product channels has been a topic of central importance to photochemistry (see refs 1–5). Few fundamental issues are typically addressed in relation to this problem: the potential energy surfaces (PES), the symmetry properties of molecular orbitals, and the nature of reaction coordinate(s). Some key questions are the following: how does the nuclear motion mediate the nonadiabatic coupling between relevant electronic states; what are the effects of intramolecular vibrational-energy redistribution (IVR); and, in the condensed phase, what is the time scale for vibrational relaxation (VR)? The rapid advance in the applications of methods of probing femtosecond dynamics and efficient electronic structure calculations are making it possible to combine these methods in studying the photochemistry of polyatomic molecules more quantitatively and in a great detail.

Of particular interest in this respect are "small" aromatic molecules that generally tend to be planar and relatively non-reactive in the electronic ground sate due to the stabilization by the strong resonance π delocalization. Optical excitation of an aromatic system into one of the lowest excited electronic states leads to promotion of one of the valence electrons into the antibonding π^* orbital. As a result, it is expected that the planar configuration of the ring may become destabilized. A few experimental and theoretical studies of benzene and aza-derivatives of benzene (azines) have suggested that, indeed, the $\pi\pi^*$ electronic excitation of the aromatic ring tends to break up the planarity (see e.g., refs 6–8). On the other hand, it is known that many of the molecules in this class, when excited with some excess energy, exhibit a very low fluorescence quantum yield due to the extremely fast nonradiative deactivation.[9–13]

It has long been speculated that the anomalously fast nonradiative relaxation and photoisomerization dynamics may be intimately connected processes.[7,8,14–18] Ever since Teller,[19]
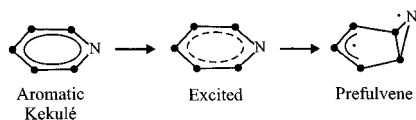
and Herzberg and Longuet-Higgins,[20] pointed out that quite frequently intersections of potential energy surfaces in poly-atomic molecules are expected to have a double-cone shape, there have been many theoretical and experimental studies of these conical intersections (CI) and their role in nonradiative, intramolecular electronic relaxation, and photochemistry.[21,22] In contrast to the well-known deactivation mechanism via internal conversion (IC), the CI, if present, would cause a much faster and more efficient passage from the initially excited reactant configuration to the different product states, leading to various isomers of the reactant or, in the simplest case, the electronic ground state.

The time scale for reactions mediated by CI is on the order of the vibrational period of the reactive mode, suggesting, depending on the specific system, a reaction time of few hundred femtoseconds. The careful distinction has to be made between the true CI characterized by crossing or near-crossing of the PESs and the avoided crossing of the PESs when there is a relatively strong interaction between two electronic configurations which leads to the formation of adiabatic states. In the latter case, slower reaction rates are expected because a nonadiabatic transition between the adiabatic states has to be involved to enable the passage from the nuclear configuration of reactants to that of products, usually described by the Landau–Zener curve crossing probability.[23,24]

The simplest of all nitrogen heterocycles[25,26] is pyridine. The photophysics and photochemistry of pyridine in the gas phase and in solution has been the subject of many theoretical as well as experimental steady-state and time-resolved studies (see refs 11, 15, 27–31). Some of the most important early findings are the following: (a) The excited electronic states at the ground-state configuration have been calculated from ab initio studies and compared with experimental values.[26] (b) Pyridine has a structureless absorption in the gas phase, especially at higher energies above the $S_1(n\pi^*)$ absorption origin (0–0 at 287.6 nm).[28–30] (c) A very low (gas phase) fluorescence ($\lambda_{max} = 330$ nm) quantum yield of ~5.9 × 10^{-5} was measured upon

Femtosecond Dynamics of Pyridine

J. Phys. Chem. A, Vol. 103, No. 37, 1999 **7409**

SCHEME 1

excitation into $S_1(n\pi^*)$ (0−0 at 287.6 nm). When exciting to $S_2(\pi\pi^*)$ (0−0 at 260.7 nm) and detecting S_1 fluorescence (there is no fluorescence from S_2), the yield is ~2.7×10^{-6}.[10,11] The direct picosecond fluorescence decay measurements yield lifetimes for S_1 from 20 to 42 ps, depending on excitation wavelength.[15,31] (d) Pyridine exhibits a relatively high intersystem crossing yield ~0.5 from $S_1(n\pi^*)$ and ~0.02 from $S_2(\pi\pi^*)$.[11,12] (e) And importantly, a photoisomerization of pyridine into Dewar-type valence isomers has been observed in solutions and matrices (with quantum yield of 1−5%) upon excitation into $S_2(\pi\pi^*)$ state.[32−35]

These findings indicate the existence of a rapid nonradiative decay processes from $S_1(n\pi^*)$ and, in particular, a very rapid nonradiative decay from the higher-energy $S_2(\pi\pi^*)$ state. A similar nonradiative relaxation, known as "channel-three" phenomenon, was observed in benzene following excitation of ~3000 cm^{-1} of excess vibrational energy above the benzene $S_1(\pi\pi^*)$ origin.[16,17,36−39] Bryce-Smith and Longuet-Higgins have suggested that a biradicalic intermediate structure called "prefulvene" might play a major role in the photoisomerization of benzene.[14] It has later been shown by semiempirical and ab initio calculations that benzene and pyrazine, at the CASSCF level, and pyridine, at the UHF level, indeed have local prefulvenic minimum correlated by the same reaction coordinate to planar configurations of these molecules in the first $S(\pi\pi^*)$ state.[6−8] Moreover, the same calculations indicated that the PES of $S(\pi\pi^*)$ state is intersected by the PES of S_0 and possibly $S_1(n\pi^*)$ (in case of pyridine) state along the same reaction coordinate.

Femtosecond time-resolved mass spectrometry and ab initio methods were recently employed by this group to study the photoisomerization dynamics of azabenzenes in the gas phase (molecular beams).[39] This work elucidated the reaction time scales and the role of conical intersections, and suggested various reactive pathways using the calculated ab initio ground-state potentials.

The dynamics of the isolated (gas phase) system is usually a starting point and often a prerequisite toward understanding the mechanism of the reaction in the condensed phase. For polar systems, the medium effect can be dramatic, manifesting itself via altered reaction rates, channels, and products. In general, at longer times, the solvent can act as energy acceptor or donor, constituting the thermal bath for the reactive system. Solvent-induced vibrational relaxation may compete with IVR by taking up part of the available total energy. Finally, the dynamic response of the solvent to changes of electronic structure during the reaction can cause stabilization of a certain transient configuration, thus altering the barrier and rates. In this case, the response time of the solvent relative to the time scale for the reaction would be an important factor. Moreover, such perturbations may cause symmetry breakdown which can alter the nonadiabatic coupling. In nonpolar solvents, such perturbations are relatively much less effective, especially at short times.

In this paper, we use femtosecond transient absorption techniques to extend the earlier gas-phase study to the condensed phase. We examine the influence of the solvent on the dynamics of isomerization and nonradiative relaxations (Scheme 1).

Time-resolved transient absorption (population and anisotropy) enables us to selectively probe the dynamics of various
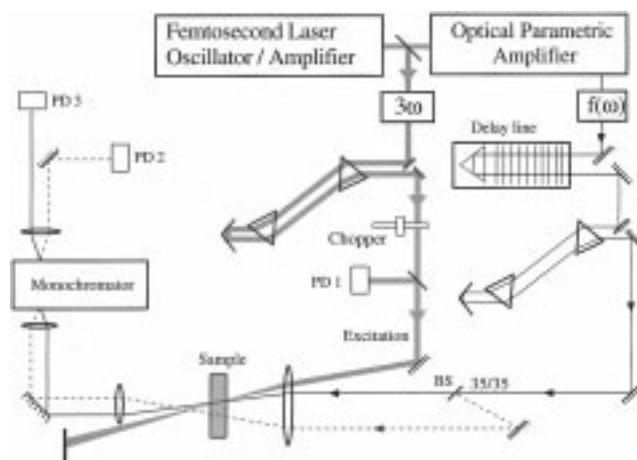

Figure 1. Experimental setup for femtosecond transient absorption.

excited states of pyridine and its high-energy isomers in solution and on the femtosecond time scale. Experiments were performed with the following focus: (i) in solvents of different viscosity and polarity (3-methylpentane, ethylene glycol, acetonitrile, and water); (ii) to examine the effects of substitution, deuteration, and protonation; and (iii) for different excitation energies. The ab initio calculations of the reaction path in the ground and excited states were performed using the CASSCF method[40,41] as well as time-dependent DFT method.[42−44] We compare theory with experiments, providing a detailed picture, which describes the deactivation and reactive pathways for the formation of the valence isomer(s).

The paper is organized as follows: in section 2, the experimental apparatus and measurement techniques are described and this is followed by presentation of the experimental results in section 3. The results of the CASSCF as well as time-dependent DFT calculations are described in section 4. Finally, in section 5, the discussion of experimental and theoretical results is given and the model is presented.

2. Experimental and Data Analysis

The transient absorption experiments were performed with a setup which is shown schematically in Figure 1. The system consists of a femtosecond (fs) Ti:sapphire oscillator coupled to a regenerative amplifier which generates 50 fs, 0.6 mJ light pulses (at 1 kHz repetition rate) tunable in the 800−840 nm wavelength range. The pulses from the amplifier were divided into two parts with a 1 to 5 ratio. The weaker beam was frequency tripled and recompressed in a double-prism configuration to provide UV excitation pulses at 266 or 278 nm with ~1 μJ per pulse. The stronger beam was used to pump an optical parametric amplifier (OPA). The output from OPO (signal or idler beam) was frequency transformed by various combinations of doubling and mixing, with the pump light at 800 nm, to produce probe pulses tunable in the broad wavelength range from 244 to 700 nm. The probe pulses were recompressed in the double-prism configuration, delayed in time with a computer-controlled delay line and divided into signal and reference beams with 35/35% beam splitter.

All three beams, *excitation*, *signal*, and *reference*, were then focused into the sample with a quartz lens ($f \approx 10$ cm), but only the excitation and signal beams were overlapped in the sample which was in a 0.3 mm spinning quartz cell. After the sample, both signal and reference beams were focused into a monochromator and detected using silicon photodiodes (PD2, PD3), which are capable of recording separately each laser pulse.
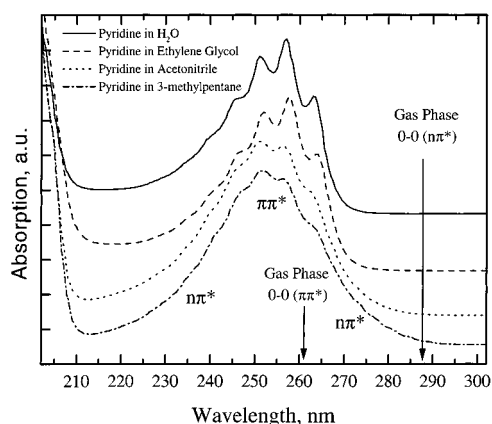
Figure 2. Steady-state absorption spectra of pyridine in different solvents. The 0−0 transitions for pyridine in the gas phase are indicated.

The chopper in the excitation beam was used to block excitation of the sample for measuring the background optical density, while photodiode PD1 was used to monitor the energy of the excitation beam and also to determine when the excitation was on and when it was off.

Typically, it was possible to measure changes of optical density on the order of 10^{-5} after averaging the signal from ∼400 pulses for each delay position. The cross-correlation function between pump and probe pulses was estimated to be ∼180 fs. The deconvolution enabled us to achieve time resolution of ∼80 fs. To examine the population dynamics, the polarization of the excitation pulse was set at the *magic angle* with respect to that of the probing pulse. The transient anisotropy was calculated from signals obtained in (∥) and (⊥) configurations according to $r(t) = (I_{\parallel} - I_{\perp})/(I_{\parallel} + 2I_{\perp})$. To rule out contributions of multiphoton processes, we have measured the pump and probe energy dependencies of the signal. At the excitation energies used to obtain all data in this work ($< 1\ \mu$J), the dependence of the signal on both pump and probe energies

was linear within 1%. At higher excitation energies (∼10 μJ) a saturation of the signal was observed.

Steady-state absorption spectra were measured on Cary 50 (Varian Inc.) spectrophotometer in a 1 cm quartz cell. HPLC grade pyridine, acetonitrile (Aldrich Inc.), and water (Em Science Inc.) were used as received. Analytic grade ethylene glycol was purchased from Mallinckrodt Inc. 2,6-Di-*tert*-butyl-4-methylpyridine (butylmethylpyridine) was purchased from Aldrich Inc. and used as received. Experiments on pyridinium ion were performed using pyridine hydrochloride obtained from Lancaster Synthesis Inc. or by adding appropriate molar amount of hydrochloric acid to pyridine solution in acetonitrile or in water. The results were identical in both cases. Conductivity experiments were performed to ensure that pyridine hydrochloride exists in ionic form in acetonitrile solution. For studies of deuteration effect pyridine-d_5, 100% D (Aldrich Inc), was used. The transient response from the sample was identical (except amplitude) in the concentration range 1.9×10^{-3} to 2.4×10^{-2} mol/L. Therefore all experiments were performed with the sample concentration of ∼2.4×10^{-2} mol/L.

Experimental data were analyzed using Scientist deconvolution software (Micromath Inc.). The ab initio calculations were performed using Gaussian 98 software, as discussed below.

3. Experimental Results

Figure 2 shows the steady-state absorption spectra of pyridine in four different solvents: water, ethylene glycol, 3-methylpentane, and acetonitrile. These spectra exhibit a few particular features which are summarized in the following: (a) a blue shift and broadening of the absorption band of the $S_1(n\pi^*)$ state as compared to the gas phase, especially in the more polar solvents, (b) sharpening of the vibronic features in the more polar and hydrogen-bonding solvents; and (c) a red spectral shift of the $S_2(\pi\pi^*)$ absorption as compared to the gas phase, which is more pronounced in the more polar solvents.
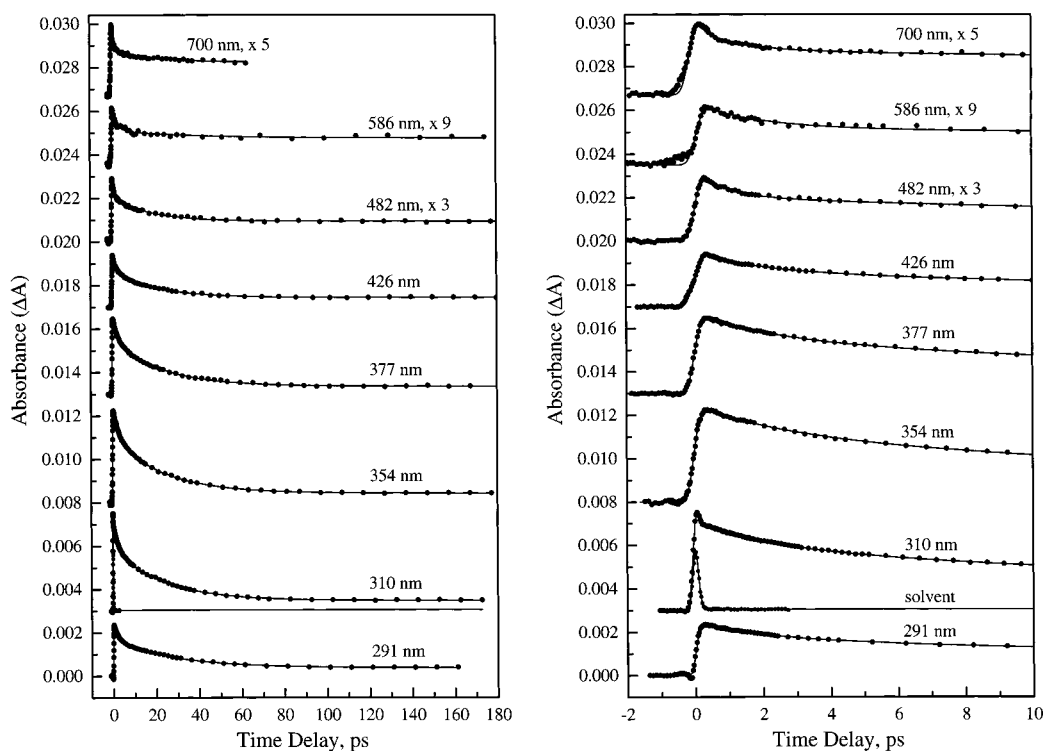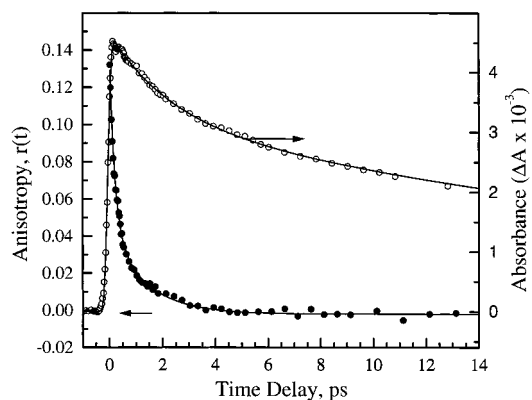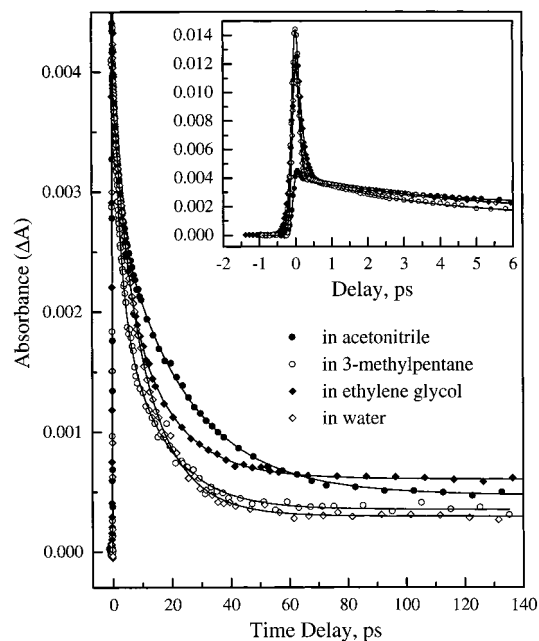

Figure 3. Femtosecond transient absorption of pyridine in acetonitrile at different probe wavelengths. Excitation was centered at 266 nm: (A, left) long-time range; (B, right) short-time range.

Femtosecond Dynamics of Pyridine

J. Phys. Chem. A, Vol. 103, No. 37, 1999 **7411**

TABLE 1: Results of Transient Absorption Analysis of Pyridine in Acetonitrile and Other Solvents: Decay Times and Amplitudes of Multiexponential Fits

τ_1, ps	τ_2, ps	τ_2, ps	A_1, %	A_2, %	A_3, %
		291 nm			
2.2	28	20000	32.3	52.1	15.6
		291 nm, Deuterated			
3.9	37	20000	28.6	53.0	18.4
	291 nm, Deuterated, τ_1 Value Fixed				
2.2	33	20000	23.0	60.0	17.0
		305 nm			
2.2	23.5	20000	30.0	57.6	12.3
		310 nm			
2.25	23.2	20000	29.1	59.2	11.7
	310 nm, in 3-Methylpentane				
2.25	14.5	20000	48.6	43.4	8.0
		310 nm, in water			
2 ± 1	9.95	20000	<14.5	78.1	7.4
	310 nm in Ethylene Glycol				
3.8	15.3	20000	36.4	48.4	15.2
		317 nm			
2	21	20000	28.2	57.4	14.3
	317 nm, in Ethylene Glycol				
3.8	15.3	20000	36.3	48.4	15.3
		354 nm			
3	23	20000	30.8	59.6	9.6
	354 nm, in Ethylene Glycol				
1.2	13	20000	25.2	60.8	14.0
		377 nm			
2.4	23	20000	32.4	57.9	9.7
		426 nm			
1.8	20	20000	34.6	48.1	17.3
		482 nm			
0.88	18	20000	36.7	33.6	29.7
		586 nm			
2	30	20000	70.5	21.7	7.8
		700 nm			
1.78	20	20000	26.0	17.7	56.3

Figure 4. Transient anisotropy of pyridine in acetonitrile, excited at 266 nm and probed at 305 nm. The magic angle population decay is also shown.

Figure 5. Transient absorption of pyridine in different solvents. λ_{exc} = 266 nm, λ_{pr} = 310 nm.

In Figure 3, A and B, we present transient absorption (TA) of pyridine in acetonitrile, excited at 266 nm and probed in the UV−vis wavelength range from 291 to 700 nm. All transients are dominated by the excited-state absorption (negative gain) except at 291 nm where a very fast, small gain signal is observed at negative delay time (appearing as a negative dip); we attribute it to coherent coupling between pump and probe pulses. The amplitude of the signal is largest in the 310−350 nm region and becomes progressively weaker at longer wavelengths. At all wavelengths, the rise of TA is instantaneous within our time resolution. Results of the fitting to superposition of exponential decay functions are summarized in Table 1. Generally, the TA decay is characterized by ∼2.2 ps, ∼23 ps, and nanosecond decay components. The relative ratio of the amplitudes of these three decay components is wavelength dependent, but the decay times remain constant (except at 482 nm, where the shortest decay time is 0.88 ps, and at 244 nm where only a 6.8 ps decay component is observed).

Figure 4 displays the transient anisotropy of pyridine in acetonitrile probed at 305 nm together with the magic-angle signal. Analysis in terms of exponential decays results in two components with the decay times of ∼200 fs and 1.3 ps. We found that the relatively high initial anisotropy (∼0.14) and ∼200 fs decay is due to the ultrafast solvent response near the zero delay time, as evidenced by experiments done with the

neat solvent. The initial value of the transient anisotropy of the pyridine itself is ∼0.04; noticeably, its decay time of ∼1.3 ps is close to the decay time of the magic angle signal (∼2.2 ps) (within the accuracy of our anisotropy experiments).

To investigate the effects of polarity and viscosity on the decays of the TA, we have performed experiments in four different solvents (see Figure 5). Quantitative analysis revealed three trends: (a) the decay constant of the short (2.2 ps) decay component is basically the same in all solvents, except in ethylene glycol, where it is increased to ∼3.8 ps; (b) the decay constant of the long time component varies significantly in different solvents (from 9.9 ps in water to 23 ps in acetonitrile); and (c) the ratio of the decay amplitudes is also wavelength dependent; for instance, the amplitude of the 2 ps component is very small in water (for more details see Table 1).

The excitation at 266 nm prepares simultaneously both the $S_1(n\pi^*)$ and $S_2(\pi\pi^*)$ states of pyridine. Therefore, we have also investigated excitation wavelength dependence (see Figure 6). Excitation into the long-wavelength shoulder of the absorption band (at 278 nm) leads to a significant reduction of the amplitude of the 2.2 ps decay component (more than 3 times), as compared to the amplitude of the 23 ps decay component, while the values of decay times remain essentially the same
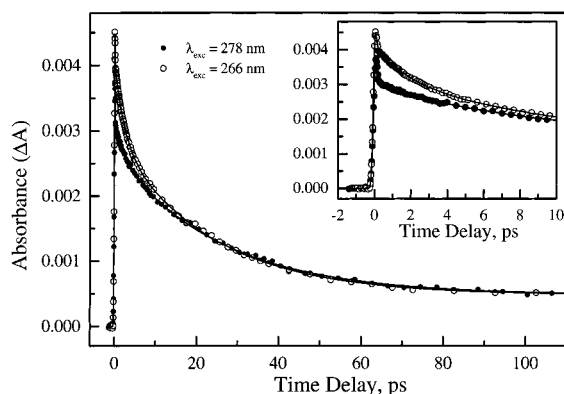
Figure 6. Transient absorption of pyridine in acetonitrile, excited at two different pump wavelengths, 266 and 278 nm.
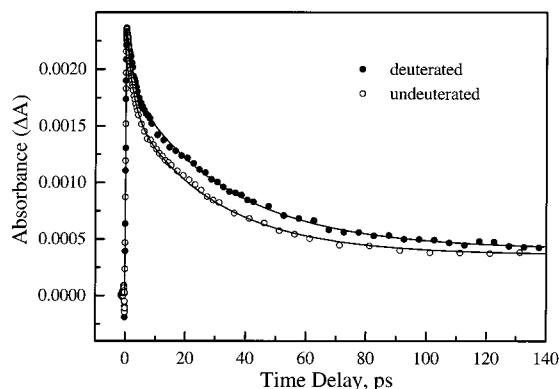

Figure 7. Transient absorption of deuterated and undeuterated pyridine in acetonitrile, probed at 291 nm. $\lambda_{exc} = 266$ nm.

($\sim$2.7 and $\sim$25 ps, $A_1 = 13.6\%$, $A_2 = 70.9\%$, $A_3 = 15.4\%$ (amplitude of nanosecond component)).

Experiments on fully deuterated pyridine indicate that the overall decay is slowed down (see Figure 7). A good fit to the data is obtained by assuming that the fast decay time ($\sim$2.2 ps) is unchanged while the decay time of the slow component is increased from 23 to 33 ps upon deuteration; the ratio of the amplitude of the slow and fast decays is also augmented from 1.85 to 2.6. If all fit parameters are allowed to vary then a 3.9 ps is obtained for the fast decay time; however, the quality of the fit is the same within accuracy of our data.

To gain further insights and disentangle the influence of the S_1 and S_2 states on the dynamics, we have chosen to study pyridinium ion
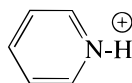
The $\pi\pi^*$ framework of states of this molecule is nearly identical to that of pyridine. However, the $n\pi^*$ states are missing in this system because the lone-pair electrons on nitrogen are expended for a formation of the covalent bond with the proton. Therefore, the lowest singlet state of pyridinium ion is $S_1(\pi\pi^*)$ state, which clearly manifests itself in the absorption spectrum through the disappearance of the absorption shoulder in the 270–290 nm region (see Figure 8). Because of this fact, our pump pulse at 266 nm can now only excite the $\pi\pi^*$ transition.

In Figure 9 we present the transient absorption of pyridinium ion in acetonitrile. The data clearly show that the slow decay component ($\sim$23 ps) is totally missing while the fast decay component remains practically unchanged ($\sim$3.3 ps in acetonitrile and $\sim$1.97 ps in water). A closer inspection of the
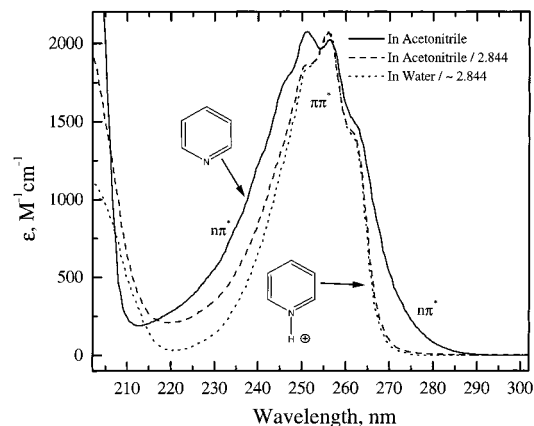

Figure 8. Comparison of steady-state absorptions of pyridinium ion (in water and acetonitrile) and pyridine in acetonitrile.
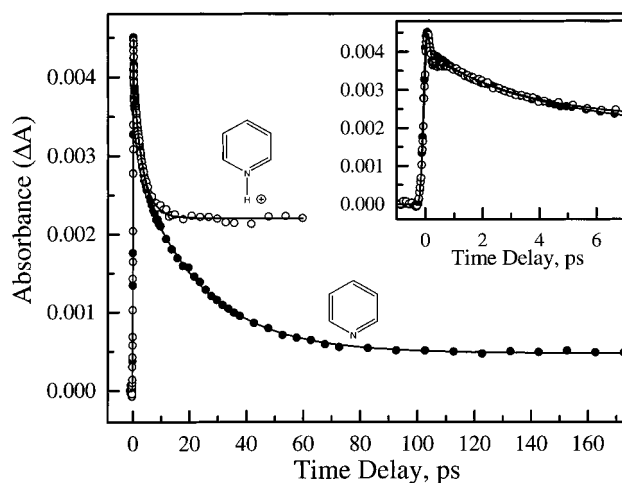

Figure 9. Transient absorption of pyridinium ion and pyridine in acetonitrile, probed at 310 nm. $\lambda_{exc} = 266$ nm.

transients reveals another difference between the TA response of pyridinium ion and pyridine (see Figure 10). In the case of pyridinium ion, the TA rise is not instantaneous: the rise time is 200 fs in acetonitrile and 310 fs in water solution. Note that the spike around zero delay time is due to the neat solvent contribution.

Finally, to investigate the effect of substituents we have performed experiments on butylmethylpyridine in acetonitrile (see Figure 11). The TA absorption signal from this molecule rises within 170 $\pm$ 70 fs and then decays to the constant background. The decay appears as a single exponential with a time constant of $\sim$9 ps; if fitted to biexponential decay, two components of $\sim$1.9 and 8.3 ps were obtained, but the amplitude of the 1.9 ps component is 11.3 times smaller than that of 8.3 ps component; this is in contrast to pyridine dynamics where this ratio is $\sim$2.

4. Ab Initio and Density Functional Theory Calculations

(A) Ground-State Absorption Spectra of Valence Isomers: Time-Dependent DFT Calculations. In an attempt to identify the structures of the absorbing species, which give rise to the TA, we have performed time-dependent (TD) DFT calculations[42–44] of the ground-state absorption spectra of valence isomers of pyridine. The geometries of Kekulé, Dewar, and Hückel structures were optimized at the RB3LYP/6-311G-(d,p) level. Subsequently, the absorption spectra were calculated at the TD DFT/6-311G(d,p) level.
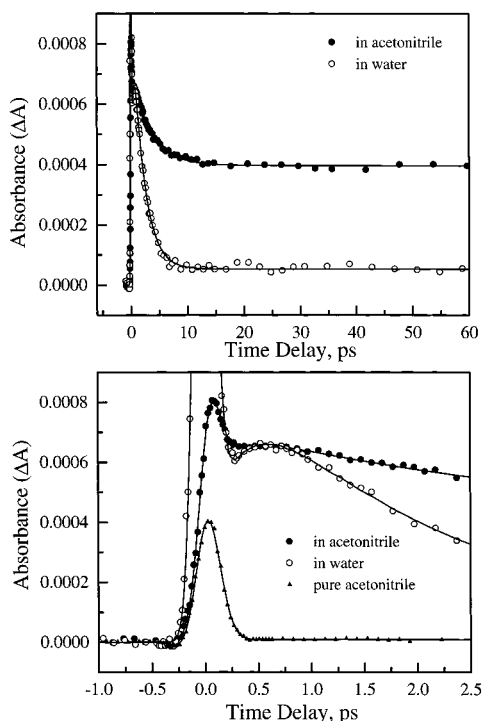
Femtosecond Dynamics of Pyridine

J. Phys. Chem. A, Vol. 103, No. 37, 1999 **7413**

Figure 10. Transient absorption of pyridinium ion in water and acetonitrile, at 310 nm. $\lambda_{exc} = 266$ nm.
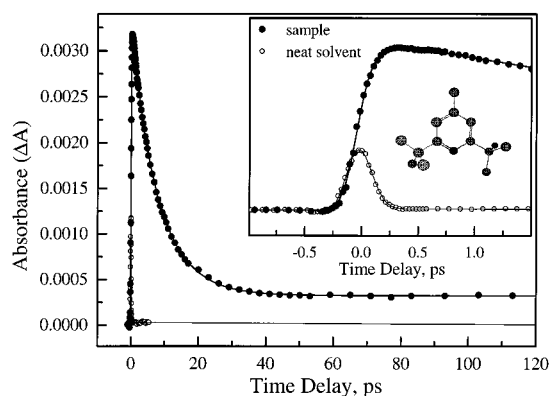

Figure 11. Transient absorption response of 2,6-di-*tert*-butyl-4-methylpyridine in acetonitrile at 310 nm, excited at 266 nm. The experimental trace was corrected for the solvent contribution.

Figure 12 displays excitation energies and oscillator strengths of six lowest singlet−singlet transitions. These results suggest that these valence isomers tend to absorb light in the same or even shorter wavelength region as compared to Kekulé (aromatic) configuration of pyridine. Intuitively, this is not a surprising result since the extent of delocalization of the π system and (π resonance) stabilization are decreasing on going from the Kekulé to the Hückel isomers; i.e., higher energy isomers are more saturated. Specifically, the Dewar isomers have two double bonds, while Hückel isomers have only one. We did not consider here the fully saturated Ladenberg-type of isomer because of its higher energy.[39] Notice that according to refs 42−44, the accuracy of excitation energies obtained using TD DFT is ∼0.4 eV. The oscillator strengths are given for the sake of comparison, but they can be much lower than the experimental values because vibronic couplings were not considered. Note that our experiments are capable of detecting absorption byproduct molecules with the oscillator strengths as low as 10^{-4}.

(B) Transition States and Conical Intersections in the Prefulvene Isomerization Path: CASSCF Calculations.
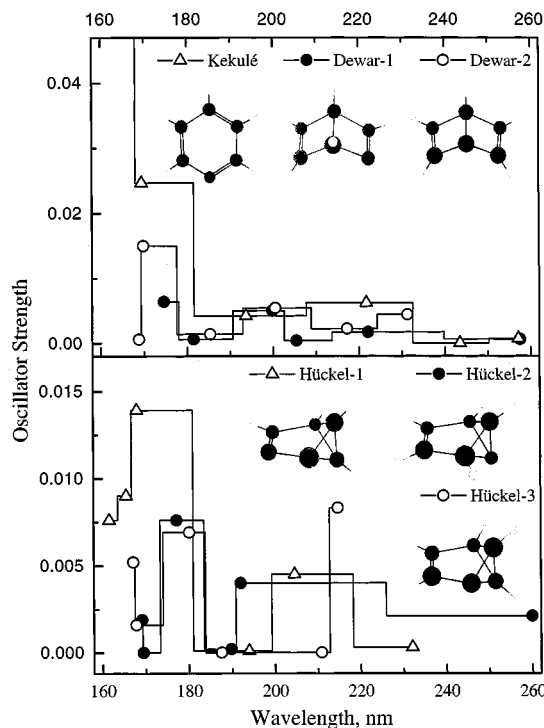

Figure 12. Results of time-dependent DFT calculations of the absorption spectra of various valence isomers of pyridine in the ground state.

Guided by previous work,[6−8,14] in this section we consider the prefulvene-type isomer for a possible isomerization reaction path of pyridine. The adequate treatment of this problem requires a method that can properly account for large electronic-structure changes along the reaction coordinate and the ability to treat near-degeneracy effects. We use complete active-space self-consistent-field method (CASSCF) which permits us to include the most important electron correlation effects by performing a full configuration interaction calculation in a limited space of active orbitals.[40,41]

In the case of pyridine, we have chosen to use the active space that consists of three occupied π orbitals, one occupied n orbital (the lone pair of nitrogen atom), and three unoccupied π^* orbitals. In the following, it will be designated by (electrons, orbitals) as (8,7), which implies that eight active electrons are distributed among seven active orbitals. In a few instances, we also used a larger space (8,8) or (10,8); however, these calculations showed that the above-mentioned space of seven orbitals is saturated in the case of pyridine, allowing us to capture the essential details relevant for the description of this system. The calculations were performed using STO-3G and 6-31G* basis sets.

In Figure 13, we show the potential energy curves of the ground state of pyridine calculated along the reaction path to the prefulvenic form. The reaction coordinate that we use is the so-called intrinsic reaction coordinate (IRC), representing the path along the lowest-energy, negative vibrational mode (saddle point) from the transition state to the reactants and products. Since symmetry breakage is involved, the clearest way to quantify this reaction path is to map out a specific set of coordinates that change monotonically along the path. The most convenient ones are the angle (α) at the nitrogen atom, defined by two bonds adjacent to nitrogen (see Figure 13), and the distance (d) between the two carbon atoms at positions 2 and 6. Values of these parameters for all relevant points on the reaction path are summarized in Table 2 and the optimized
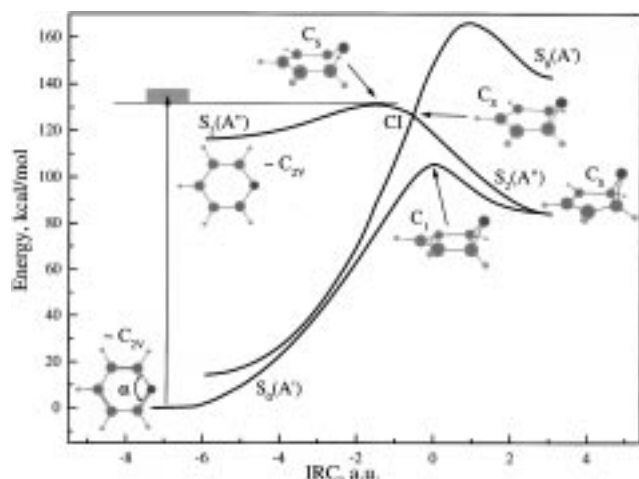
Figure 13. Calculated potential energy surfaces of pyridine. The reaction path was optimized at the CASSCF(8,7)/STO-3G level of theory. The lowest-energy path represents the adiabatic reaction path on the ground state. The $S_2(A'')$ path is the lowest energy path on the $S_2(\pi\pi^*)$ potential energy surface, while the higher $S_0(A')$ represents the energy of the S_0 state along this path at the vertical transition energy.

TABLE 2: Calculated Values, CASSCF(8,7)/6-31G*, of the Angle α at the Nitrogen Atom Which Forms Two Bonds to the Carbon Atoms at Positions 2 and 6, and the Distance d between These Two Carbon Atoms for Four Different Conformations of Pyridine

geometry	α, deg	d, Å
Kekulé$-S_0$, C_{2v}	114.8	2.321
Kekulé$-S_2$, $\sim C_{2v}$	112.8	2.388
transition state, $S_2(\pi,\pi^*)$, C_s	91.8	2.103
conical intersection, S_0-S_2, C_s	80.9	1.903
transition state, S_0, C_1	69.4	1.643
prefulvene, S_0, C_s	55.7	1.478

geometries are shown in Figure 14. Similar calculations were made for the $S_2(\pi\pi^*)$ excited state. More detailed discussion of these results will be provided in the discussion section. It must be emphasized that within the level of ab initio theory used here, the energies of the excited states can easily be off by $\sim$10 kcal/mol. Notice that at this level, the $n\pi^*$ state lies at higher energies than the lowest $\pi\pi^*$ state, but the accurate energy position is not our focus here.

(C) Ground-State Absorption of Prefulvene. In Figure 15, we present the singlet$-$singlet absorption spectra of the prefulvene isomer, calculated at the TD DFT B3LYP/6-311G(d,p) and CASSCF(8,7)/6-31G* levels. Notice the presence of numerous states with excitation energies falling into a broad range from near-UV to infrared. Although oscillator strengths of the lowest energy transitions are near zero, the solvent environment and vibronic coupling between electronic states is very likely to lead to intensity borrowing and distortion of C_s symmetry of prefulvene, thus resulting in finite absorption in a broad wavelength range.

(D) Geometry and Emission Spectrum of Pyridine $S_1(n,\pi^*)$ State. It has been pointed out earlier that, at least in the triplet $n\pi^*$ state, pyridine assumes a "boat" type geometry.[6] The treatment of this kind of geometry, using the CASSCF method, requires inclusion of a large number of mixed n and π orbitals. Upon trial it was found to converge slowly with our available computation speed. Therefore, we have optimized the geometry of this state using the single-excitation configuration interaction method, CIS/6-311G(d,p). Subsequently, we calculated vertical emission energies using the TD DFT/6-311G(d,p) method. The results of the structure and spectra presented in Figure 16
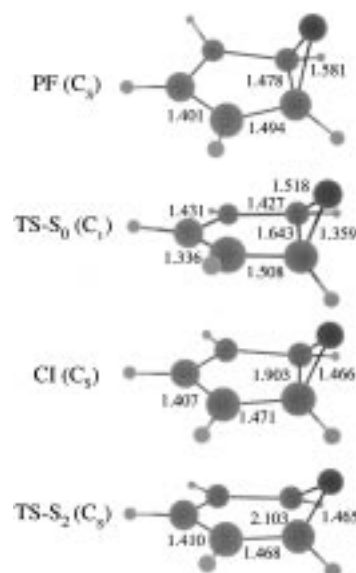

Figure 14. Geometries of the pyridine molecule at the transition state (TS), in prefulvenic form (PF) and at the conical intersection (CI). The PF and TS geometries are optimized at the CASSCF(8,7)/6-31G* level of theory, while the CI geometry is optimized at the CASSCF(8,7)/ STO-3G level.
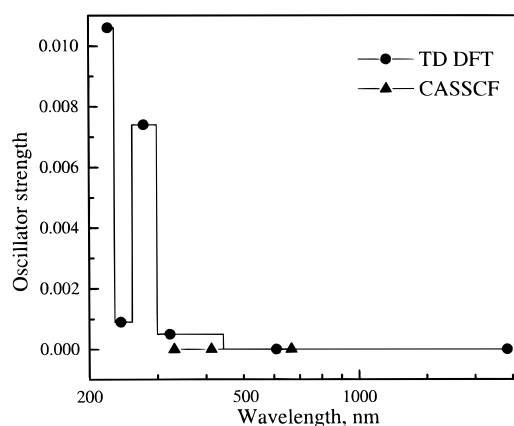

Figure 15. Calculated absorption of the prefulvene structure. Spectra were calculated at the TD DFT B3LYP/6-311G(d,p) and CASSCF-(8,7)/6-31G* levels of theory.

indicate that pyridine has a nonplanar, boat-shaped geometry and that the lowest electronic transition is shifted to lower energies by approximately 7000 cm^{-1}. Within the accuracy of the approximations used, this value agrees with the experimentally observed fluorescence Stokes shift.[11]

5. Discussion

(A) Time Scales and Dynamics. There are four key observations which enable us to paint a total picture for the dynamics. First, the excitation to the lowest state ($S_1(n\pi^*)$) showed the 23 ps component with the first component (2.2 ps) drastically reduced; excitation to the $S_2(\pi\pi^*)$, on the other hand, shows a pronounced 2.2 ps component besides the slow one of 23 ps. In what follows we shall refer to the $\sim$2.2 ps as the fast component and the $\sim$23 ps as the slow one. Second, the pyridinium ion, where the $n\pi^*$ transition is absent, shows only the fast component. Third, in the four solvents we studied, the fast component is essentially robust, but the slow one changes with polarity, viscosity, and hydrogen-bonding ability. Fourth, the fast component is present for both deuterated and undeuterated pyridine, but it almost disappears in the butylmethylpy-
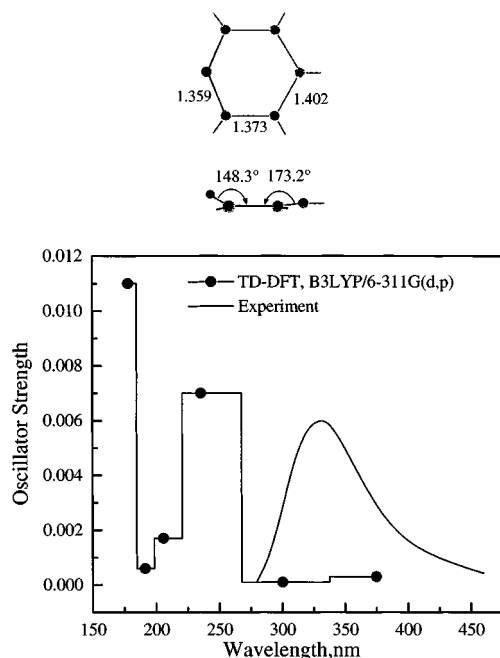
Femtosecond Dynamics of Pyridine

J. Phys. Chem. A, Vol. 103, No. 37, 1999 **7415**

Figure 16. Geometry and emission spectrum of pyridine in the S_1-($n\pi^*$) state calculated using the TD DFT B3LYP/6-311G(d,p) method. The experimental fluorescence spectrum (ref 10) is also shown.
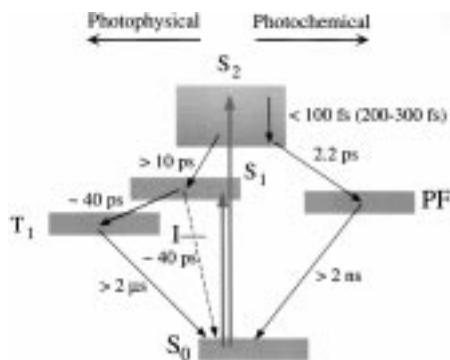

Figure 17. Energy-level schematics and time scales for the photochemical and photophysical processes discussed in text.

ridine. Accordingly, the fast decay results from motion on the $\pi\pi^*$ reaction path to form isomers, while the slow one represents, after $S_2 \rightarrow S_1$ relaxation, the nonradiative, nonreactive pathway of S_1, mostly by the intersystem crossing to the triplet, as discussed below. The picture is elucidated by the energy-level diagram in Figure 17. To the left, we show the standard nonradiative decay channels and to the right the reactive path for isomer formation.

The first point we address is the initial motion of the wave packet that is prepared with vibrational excess energy on the global PES. The motion which leads to bifurcation is on the femtosecond time scale.[39] We were not able to directly detect the rise of the TA signal from pyridine because of the interference from solvent contribution to the signal near the zero delay time (notice that this rise may also escape detection in the case when the TA of the initially excited state has a similar amplitude to that of TA of the final state). In pyridine such rise must be less than 100 fs. However, in the case of butylmethylpyridine and pyridinium ion we do observe the finite rise of the transient absorption signal (200−300 fs). The rise, of course, contains any perturbation by the solvent, but on such femtosecond time scale the significant effect is that of the relevant nuclear motion since the molecule becomes much less bonding in the excited state.

The observed excitation wavelength dependence enables us to assign the ∼23 ps decay component to the dynamics of the $S_1(n\pi^*)$ state. On the other hand, the TA of the pyridinium ion lacks the 23 ps component, indicating that a 2.2 ps component must originate from the pyridine excited $S_2(\pi\pi^*)$ state (which is the $S_1(\pi\pi^*)$ in the case of pyridinium ion). This conclusion is also supported by the lack of fluorescence from S_2 (in the gas phase) and by the deduced nonradiative decay rate of ∼1 ps at our excitation energy from knowledge of the quantum yield (see Figure 9 of ref 11). It should be noted that this fast nonradiative decay, taken to be the $S_2 \rightarrow S_1$ conversion in ref 11, is due to the reactive channel since, as mentioned before, it is present in the pyridinium species and absent when we excite to S_1. Thus, the ∼2.2 ps decay describes the photochemical pathway from the S_2 state. We also observe a long-lived (on our time scale) TA, which, therefore, suggests that the lifetime of the nascent PF is >2 ns. In a matrix and at longer lifetimes it is possible that prefulvene serves as an intermediate for further conversion to Kekulé or other isomers.[32−35]

Upon excitation to S_1 the amplitude of the 2.2 ps decay is reduced to a zero value and we see only the ∼23 ps decay. Also, we observe a background TA, which is similarly consistent with triplet−triplet absorption from the long-lived T_1 state after intersystem crossing.[12] It is known that the intersystem crossing yield (ISC) from the $S_1(n\pi^*)$ state is ∼0.4−0.5 in the gas phase, resulting in a ISC rate constant of ∼38 ps;[11,12] the radiative lifetime of S_1 is ∼333 ns ($f = 0.003$). Such a nonradiative rate is expected for $^1(n\pi^*) \rightarrow {}^3(\pi\pi^*)$, based on El-Sayed's rules.[45] On the other hand, in the case of pyridinium ion the ISC rate should be much slower than the observed 2.2 ps since $^1(\pi\pi^*) \rightarrow {}^3(\pi\pi^*)$ transitions are forbidden to a first order.[45]

The internal conversion rate between S_2 and S_1 states cannot be faster than the observed decay of the S_2 state (2.2 ps). Our measurements of the decay in pyridinium ion give an estimate of the total decay rate for the formation of the PF and the IC to S_0 (there is no lower $n\pi^*$ state). Knowing the rate for S_2 of pyridine and the fluorescence quantum yields of S_1 and S_2, we then estimate the IC from S_2 to S_1 to be on the order of ∼10 ps. The fact that the rate of decay of pyridinium ion did not change very significantly from that of pyridine indicates that the $S_2 \rightarrow S_1$ channel must be slower than that leading to formation of prefulvene.

To complete the picture described above, the species designated "PF" in Figure 17 is the prefulvenic form of pyridine. We base this assignment on the following points: (1) The energy of prefulvene is lower than that of the initially excited $S_2(\pi^*)$ state (see section 4). (2) It is an isomer of pyridine in the accessible energy range that may have numerous absorption bands in the broad wavelength range from UV to IR, as indicated by the quantum calculations (see section 4). (3) The $S_2(\pi^*)$ state of pyridine correlates with the ground state of prefulvene (see section 4). In Figure 18, we present the dynamics, using the theoretically calculated PES of pyridine, and the experimentally observed time scales.

(B) Deactivation Pathways of S_2 Excited State. Our ab initio PES, presented in Figure 13, shows that the isomerization path to the prefulvene is different in the ground and excited (S_2-(π^*)) states of pyridine. The adiabatic ground-state path has a high-energy barrier (112 kcal/mol) which is caused by (a) the energy loss due to reduced resonance π stabilization of the aromatic Kekulé structure and (b) subsequent stabilization on the product side due to formation of the σ bond between the carbon atoms at the 2 and 6 positions. Remarkably, the passage to the product side also involves a significant change in
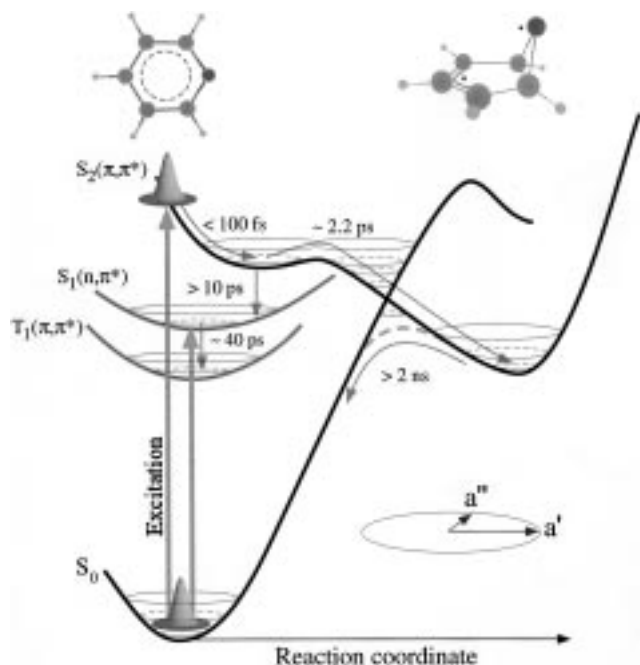
Figure 18. A schematic of potential energy surfaces representing the photochemistry and photophysics of pyridine in solution. The reaction coordinate to prefulvene is along the a′ symmetry, while a″ is the perpendicular distortion; both define the conical intersection shown. Reaction coordinates for other isomers are not shown.

symmetry at the transition state, which has a C_1 symmetry. This is caused by the antisymmetric (a″) distortion of the pyridine molecule which couples the $S_0(A')$ ground state with the S_2-(A″) excited state. The resulting interaction lowers the energy of the transition state by pushing these two states away, effectively reducing the barrier height for the ground-state isomerization (Figure 13).

Excitation of the pyridine into the $S_2(\pi\pi^*)$ state leads to a significant reduction of the aromatic stabilization since one electron is promoted into the antibonding π^* orbital. However, our calculations indicate that the pyridine molecule is still planar in the $S_2(\pi\pi^*)$ state, unlike the geometry in $S_1(n\pi^*)$; only the bond distances become larger due to less bonding character of the $S_2(\pi^*)$ state. As can be seen in Figure 13, the barrier height for isomerization to the prefulvene is significantly reduced (to <14 kcal/mol) since much less energy is required to break up the planarity in this case. In contrast to the ground state, in $S_2(A'')$, the lowest energy reaction path *conserves* the C_s symmetry all the way to the prefulvenic form. The underlying reason for this is that any antisymmetric distortion of the pyridine would increase the energy of the excited state by inducing coupling between $S_2(A'')$ and $S_0(A')$ states. This is especially true near the crossing point of the PES of $S_2(A'')$ and $S_0(A')$ states. Thus, it is natural to assume that upon photoexcitation into the S_2 state the pyridine molecule will choose the lowest energy path which is symmetric and intersects with the ground state.

It is apparent that the intersection encountered here has a conical shape since along the reaction path the two potentials have different symmetry but any orthogonal a″ distortion of the pyridine will lead to the repulsion of the adiabatic PES, because A′ × a″ × A″ = A′. This situation is reminiscent of the conical intersections discussed by Teller, Herzberg, and Longuet-Higgins,[19,20] with the difference that in the case of pyridine the intersecting states have different symmetry and nondiagonal coupling is *introducing* the repulsion between relevant electronic states. The PES obtained by us in this work

are similar to those obtained by Sobolewski et al.[8] for benzene and pyrazine, which may be expected since the $S_2(\pi^*)$ of pyridine is of the same nature as the $S_1(\pi^*)$ state of benzene. Another important result is that the ground state of the prefulvenic pyridine has A″ symmetry which is due to the fact that the prefulvene is a biradicaloid system. This is also one of the reasons why its lowest electronic transitions are strongly shifted to lower energies.

Based on the above discussion, the following picture emerges for the photoisomerization of pyridine. Initial excitation with the femtosecond light pulse prepares the pyridine molecule in a nonequilibrated S_2 state with some excess energy (see Figure 18). With time, the molecule begins to acquire the equilibrium geometry of the S_2 state by structural relaxation which is represented by the initial wave packet motion in Figure 18. According to our estimates this process takes less than 100 fs in the case of pyridine. However, in the case of butylmethylpyridine, which is much bulkier, and in the case of the pyridinium ion species, which is strongly solvated due to its positive charge, this initial process is slowed to ~170 fs (in 3-methylpentane) and 210−310 fs (in acetonitrile and water), respectively. The bulkiness and stiffness apparently hinder the structural relaxation, which on such time scales is weakly solvent dependent.

In the next step, pyridine isomerizes into prefulvene by going over the barrier in the S_2 state and crossing the conical intersection. The overall process takes ~2.2 ps and this decay time is weakly dependent on the solvent. Since the CI occurs within the time scale of the vibrational period (along the PF reaction coordinate) the observed 2.2 ps time must reflect the involvement of other coordinates in the barrier crossing process. Notice that this behavior is an isolated molecule dynamics. It is also possible that solvent fluctuations might introduce transient a″ distortions of the molecule thus leading to transient avoided crossing between S_2 and S_0 and resulting in a slower passage to the prefulvene product because of the increased finite probability of recrossing to the ground state of the aromatic Kekulé geometry. According to this picture of molecular isomerization, we do not expect significant changes of the isomerization rate upon deuteration or in different solvents, which is confirmed by the experimental observations. Because ~46 kcal/mol of energy are released in this reaction, subsequent vibrational cooling of the prefulvene may account for some variation of the fast decay component observed by probing at different wavelengths (see Table 1).

Additional confirmation of the picture comes from analysis of transient anisotropy experiments which indicate that the initial TA anisotropy is very low (0.04) and decays to zero value in ~1.3 ps. In the case of the aromatic Kekulé geometry of pyridine (C_{2v}), the direction of the transition dipole moments between different electronic states can only be parallel or perpendicular (for the ∥ case, the initial anisotropy is 0.4 while for the ⊥ case it is −0.2). Thus, the very small, experimentally observed decay of anisotropy from 0.04 to 0 is consistent with the major change in symmetry along the reaction path.

The amplitude of the 2.2 ps decay component is drastically reduced and almost undetectable in the case of pyridine in water and in the case of butylmethylpyridine in 3-methylpentane. This behavior is also consistent with the idea of bifurcation of the wave packet. Due to the strong solvent or steric effect the efficiency of the PF reactive path decreases and a relatively faster internal conversion occurs between S_2 and S_1 states of pyridine. It is known that polar, and especially hydrogen-bonding solvents, can noticeably change the gap between the $n\pi^*$ and $\pi\pi^*$ state thus leading to faster rate of ISC (vide infra).

Femtosecond Dynamics of Pyridine

J. Phys. Chem. A, Vol. 103, No. 37, 1999 **7417**

Finally, on the time scale of our experiments (up to 1 ns) we did not detect any slow decay of the background TA signal which reflects the slow rate of the rearomatization (or interconversion to other isomers) of the molecule. Calculations indicate that the barrier for this reaction in the gas phase is >21 kcal/mol (see section 4); however, it may be even higher in the solvent due to additional stabilization of prefulvenic configuration (e.g. via formation of the zwitterionic state).

(C) The Photophysical Pathway. The slow (~23 ps) decay component reflects the ISC process from the $S_1(n\pi^*)$ state, as discussed above. The triplet−triplet absorption spectrum of pyridine in the vapor phase was measured in 282−323 nm wavelength region by Selco et al.[12] In this region, the spectrum is a monotonically decreasing function of wavelength. It is expected that triplet−triplet absorption may extend even to much longer wavelengths because of the presence of closely located excited triplet states.[27]

The ISC yield can be as high as ~0.5 upon excitation into the 0−0 transition of $S_1(n\pi^*)$ state in the gas phase. It is likely that in nonpolar solvents the ISC quantum yield may remain the same as in the gas phase. Accordingly, the observed total rate of $(23 \text{ ps})^{-1}$ indicates that $k_{ISC} \sim (46 \text{ ps})^{-1}$. The other nonradiative channel (with the other 0.5 quantum yield) is the decay to the ground state (IC) and conversion to PF and other isomers (see Figures 17 and 18). The isomerization in the S_1 state is also suggested by the earlier UHF calculations by Sobolewski and Domcke,[7] which revealed a crossing point between the PES of $S_1(n\pi^*)$ and $S_2(\pi\pi^*)$. This is also consistent with the gas-phase results,[39] recognizing that the effective barrier may be different in solutions.

The interplay of these two nonradiative deactivation mechanisms of S_1 state is likely to be the cause of the spectral variation of the relative amplitude of the slow decay components observed in the experimental TA decays and probed at various wavelengths. Moreover, the solvation process of the $n\pi^*$ and $\pi\pi^*$ states is expected to lead to significant variation of the two nonradiative deactivation rates discussed above, since it is believed that the energy gap between $S_1(n\pi^*)$ and $S_2(\pi\pi^*)$, and $S_1(n\pi^*)$ and $T(\pi\pi^*)$ states may vary significantly in solvents of different polarity.[46]

From our calculations, the permanent dipole moment of pyridine in the ground state is ~2.15 D, in close agreement with the experiment result of 2.36 D.[47] This value is reduced to ~0.6 D in the $S_1(n\pi^*)$ state while in $S_2(\pi\pi^*)$ it is ~1.8 D, according to the calculations. It has been shown that the blue shift of $S_1(n\pi^*)$ transition in the solutions can be successfully simulated using reaction field theory, i.e., the change in dipole solvation, not due to the conventional picture of hydrogen bonding.[48] In solvents like water, there is an additional contribution to the blue shift because the energy of the lone pair orbital is lowered as a result of the hydrogen bond formation with water molecules, while the π^* orbital energy remains relatively unaffected.

6. Conclusion

In this work, we have combined femtosecond transient absorption spectroscopy with electronic structure methods to study excited-state deactivation pathways of pyridine in the condensed phase. The experiments show the distinct dynamics of $S_1(n\pi^*)$ and $S_2(\pi\pi^*)$ states. The benzene-like $S_2(\pi\pi^*)$ state of pyridine is reactively deactivated in ~2.2 ps. Using ab initio methods we calculated the PES of $S_2(\pi\pi^*)$ and S_0 states and found a *conical intersection* between these two states. We further showed that the $S_2(\pi\pi^*)$ excited state correlates to the ground

state of the prefulvenic form of pyridine identified as a main product in the reaction from S_2. The formation of the prefulvenic form proceeds via two-step mechanism in ~2.2 ps: at first, the system structurally relaxes in a few 100 fs or less and then crosses the barrier toward the conical intersection to reach the ground state of prefulvene.

The nonradiative deactivation of the $S_1(n\pi^*)$ excited state of pyridine occurs in 9−23 ps, depending on the solvent. There are two channels for the decay, the intersystem crossing to the $T(\pi\pi^*)$ triplet state (based on the high ISC yield and the spectral properties of triplet−triplet absorption), and the interconversion to other isomers. Earlier theoretical study has indicated that the PES of the $S_1(n\pi^*)$ and $S_2(\pi\pi^*)$ states have a crossing point along the isomerization coordinate to prefulvene,[7] but the barrier is too high for the S_1 population to interconvert to prefulvene. However, the S_1 interconversion to other isomers (Dewar's, Hückel's, etc.), which involves different type of motion from that of prefulvene formation, is possible and the rate is dependent on the relative energy of S_1 to the ground-state barrier height(s).[39] In S_2 the conical intersection is facilitated by the planar expansion, similar to the case of azulene.[49] On the other hand, in S_1, the nonplanar geometry requires other large-amplitude motions for forming isomers (other than prefulvene, which has high-energy barrier in the S_1 state) and these may be hindered in the condensed phase, hence the bias toward the photophysical route.

The solvent plays a role in the observed dynamics by introducing relative shifts of the energy levels and acting as a thermal bath. This follows from the comparison with the earlier work from this group on femtosecond dynamics of azines in the gas phase, which reveals a bifurcation of the wave packet to the reactive (by CI) and nonreactive (IC) channels, and the sensitivity of the branching to the time scale of the nuclear motions relative to the total decay time.[39] The solvent changes this branching of trajectories depending on energetics and frequencies which are controlled by polarity and viscosity. The time scale of the solvent motion relative to that of the passage through the transition state of CI is what determines the dynamics.

We have also studied other azines (and benzene), namely pyrimidine and triazine, in acetonitrile. Remarkably, we observe the fast decay component but the slow (tens of picoseconds) component changes noticeably, triazine being the longest and pyridine the shortest. These studies are important for generalization of the bifurcation concept and is directly relevant to the isomerization dynamics of one azine to another (e.g. pyrazine to pyrimidine), a subject which has been studied for many years.[50,51]

References and Notes

(1) Klessinger, M.; Michl, J. *Excited states and photochemistry of organic molecules*; VCH: New York; 1995, and references therein.

(2) Butler, L. J. *Annu. Rev. Phys. Chem.* **1998**, *49*, 125.

(3) Woodward, R. B.; Hoffmann, R. *The Conservation of orbital symmetry;* Verlag Chemie and Academic Press: New York, 1970.

(4) Baer, T.; Hase, W. L. *Unimolecular Reaction Dynamics*; Oxford University Press: New York, 1996, and references therein.

(5) Harris, A. L.; Brown, J. K.; Harris, C. B. *Annu. Rev. Phys. Chem.* **1988**, *39*, 341.

(6) Nagaoka, S.-I.; Nagashima, U. *J. Phys. Chem.* **1990**, *94*, 4467.

(7) Sobolewski, A. L.; Domcke, W. *Chem. Phys. Lett.* **1991**, *180*, 381.

(8) Sobolewski, A. L.; Woywod, C.; Domcke, W. *J. Chem. Phys.* **1993**, *98*, 5627.

(9) Lim, E. C. *Adv. Photochem.* **1997**, *23*, 165, and references therein.

(10) Yamazaki, I.; Baba, H. *J. Chem. Phys.* **1977**, *66*, 5826.

(11) Yamazaki, I.; Sushida, K.; Baba, H. *J. Chem. Phys.* **1979**, *71*, 381.

(12) Selco, J. I.; Holt, P. L.; Weisman, R. B. *J. Chem. Phys.* **1983**, *79*, 3269.

(13) Avouris, P.; Gelbart, W. M.; El-Sayed, M. A. *Chem. Rev.* **1977**, *77*, 794, and references therein.

(14) Bryce-Smith, D.; Longuet-Higgins, H. C. *Chem. Commun.* **1966**, *17*, 593.

(15) Yamazaki, Y.; Murao, T.; Yamanaka, T.; Yoshihara, K. *Faraday. Discuss. Chem. Soc.* **1983**, *75*, 395.

(16) Sobolewski, A. L. *J. Chem. Phys.* **1990**, *93*, 6433.

(17) Callomon, J. H.; Parkin, J. E.; Lopez-Delgado, R. *Chem. Phys. Lett.* **1972**, *13*, 125.

(18) Phillips, D.; Lemaire, J.; Burton, C. S.; Noyes, W. A., Jr. *Adv. Photochem.* **1968**, *5*, 329.

(19) Teller, E. *J. Phys. Chem.* **1937**, *41*, 109.

(20) Herzberg, G.; Longuet-Higgins, H. C. *Trans. Faraday Soc.* **1963**, *35*, 77.

(21) Bernardi, F.; Olivucci, M.; Robb, M. A. *Chem. Soc. Rev.* **1996**, *25*, 321.

(22) Yarkony, D. R. *Acc. Chem. Res.* **1998**, *31*, 511, and references therein.

(23) Landau, L. D. *Phys. Sov. Union* **1932**, *2*, 46.

(24) Zener, C. *Proc. R. Soc. London* **1932**, *137A*, 696.

(25) Innes, K. K.; Ross, I. G.; Moomaw, W. R. *J. Mol. Spectrosc.* **1988**, *132*, 492, and references therein.

(26) Fulscher, M. P.; Andersson, K.; Roos, B. O. *J. Phys. Chem.* **1992**, *96*, 9204, and references therein.

(27) Hoover, R. J.; Kasha, M. *J. Am. Chem. Soc.* **1969**, *91*, 6510.

(28) Bolovinos, A.; Tsekeris, P.; Philis, J.; Pantos, E.; Andritsopoulos, G. *J. Mol. Spectrosc.* **1984**, *103*, 240.

(29) Villa, E.; Amirav, A.; Lim, E. C. *J. Phys. Chem.* **1988**, *92*, 5393.

(30) Mochizuki, Y.; Kaya, K.; Ito, M. *J. Chem. Phys.* **1976**, *65*, 10.

(31) Yamazaki, I.; Murao, T.; Yoshihara, K.; Fujita, M.; Sushida, K.; Baba, H. *Chem. Phys. Lett.* **1982**, *92*, 421.

(32) Wilzbach, K. E.; Raush, D. J. *J. Am. Chem. Soc.* **1970**, *92*, 2178.

(33) Chapman, O. L.; McIntosh, C. L.; Pacansky, J. *J. Am. Chem. Soc.* **1973**, *95*, 614.

(34) Ratajczak, E.; Sztuba, B. *J. Photochem.* **1980**, *13*, 233.

(35) Johnstone, D. E.; Sodeau, J. R. *J. Phys. Chem.* **1991**, *95*, 165.

(36) Schuyler, M. W.; Parmenter, C. S. *Trans. Nonrad. Mol.*, *20th Reun. Soc. Chem. Phys.* **1970**, 92 (suppl. to *J. Chem. Phys.*).

(37) Shubert, U.; Riedle, E.; Neusser, H. J.; Shlag, E. W. *J. Chem. Phys.* **1986**, *84*, 6182, and references therein.

(38) Bryce-Smith, D.; Gilbert, A. *Tetrahedron* **1976**, *32*, 1309.

(39) Zhong, D.; Diau, E. W.-G.; Bernhardt, T.; De Feyter, S.; Roberts, J. D.; Zewail, A. H. *Chem. Phys. Lett.* **1998**, *298*, 129.

(40) Roos, B. O. *Acc. Chem. Res.* **1999**, *32*, 137, and references therein.

(41) Roos, B. O. in *Ab Initio Methods in Quantum Chemistry*; Lawley, K. P., Ed.; Wiley: New York, 1987; Vol. II, p 399.

(42) Bauernschimitt, R.; Ahlrichs, R. *Chem. Phys. Lett.* **1996**, *256*, 454.

(43) Casida, M. E.; Jamorski, C.; Salahub, D. R. *J. Chem. Phys.* **1998**, *108*, 4439.

(44) Bauernschimitt, R.; Ahlrichs, R.; Hennrich, F. H.; Kappes, M. M. *J. Am. Chem. Soc.* **1998**, *120*, 5052.

(45) El-Sayed, M. A. *J. Chem. Phys.* **1963**, *38*, 2834.

(46) Eisenthal, K. B.; Moss, R. A.; Turro, N. J. *Science* **1994**, *225*, 1439.

(47) DeMoore, B. B.; Wilcox, W. S.; Goldstein, J. H. *J. Chem. Phys.* **1954**, *22*, 876.

(48) Karelson, M.; Zerner, M. C. *J. Am. Chem. Soc.* **1990**, *112*, 9405.

(49) Diau, E. W.-G.; De Feyter, S.; Zewail, A. H. *J. Chem. Phys.* **1999**, *110*, 9785.

(50) Lahmani, F.; Ivanoff, N. *J. Phys. Chem.* **1972**, *76*, 2245.

(51) Lahmani, F.; Frad, A.; Tramer, A. *Chem. Phys. Lett.* **1972**, *14*, 337.